GEOCHEMISTRY

Garnet petrochronology reveals the lifetime and dynamics of phonolitic magma chambers at Somma-Vesuvius

Jörn-Frederik Wotzlaw[1]*, Lena Bastian[1], Marcel Guillong[1], Francesca Forni[2], Oscar Laurent[1,3], Julia Neukampf[1,4], Roberto Sulpizio[5,6,7], Cyril Chelle-Michou[1], Olivier Bachmann[1]

Somma-Vesuvius is one of the most iconic active volcanoes with historic and archeological records of numerous hazardous eruptions. Petrologic studies of eruptive products provide insights into the evolution of the magma reservoir before eruption. Here, we quantify the duration of shallow crustal storage and document the evolution of phonolitic magmas before major eruptions of Somma-Vesuvius. Garnet uranium-thorium petrochronology suggests progressively shorter pre-eruption residence times throughout the lifetime of the volcano. Residence times mirror the repose intervals between eruptions, implying that distinct phonolite magma batches were present throughout most of the volcano's evolution, thereby controlling the eruption dynamics by preventing the ascent of mafic magmas from longer-lived and deeper reservoirs. Frequent lower-energy eruptions during the recent history sample this deeper reservoir and suggest that future Plinian eruptions are unlikely without centuries of volcanic quiescence. Crystal residence times from other volcanoes reveal that long-lived deep-seated reservoirs and transient upper crustal magma chambers are common features of subvolcanic plumbing systems.

INTRODUCTION

Volcanic hazards threaten the lives of millions of people worldwide. The most violent eruptions produce widespread ash falls and pyroclastic flows that can destroy entire cities far beyond the slopes of the volcanic edifice. Somma-Vesuvius, an active stratovolcano located in the Campanian Plain (Southern Italy), has a remarkably well-preserved record of hazardous eruptions because of written documents of Roman and Christian chroniclers and archeological excavations (*1*–*4*). The eruption of AD 79 is the most prominent in the volcano's history as it was documented in detail by Pliny the Younger and buried the Roman cities of Pompeii and Herculaneum (*1*, *2*). The volcanological record provides evidence for several similar explosive eruptions including a total of four large Plinian and several sub-Plinian events during the past ~22,000 years (*5*, *6*). Juvenile pyroclasts and the crystal cargos of erupted products provide insights into the pre-eruption storage conditions (*7*, *8*), magma ascent paths (*9*, *10*), and potential eruption triggers (*11*). Magma storage conditions are further constrained experimentally, suggesting progressive upward migration of the magma chamber beneath Somma-Vesuvius, consistent with pressure estimates based on geochemical data (*12*, *13*).

However, the lifetime of the eruption-feeding magma chambers and the processes from magma chamber assembly to eruption remain poorly constrained. This is largely due to the absence of actinide-rich accessory minerals such as zircon and allanite that have been used at other active and dormant volcanoes to quantify the time scales of pre-eruption upper crustal magma storage using U-series dating (*14*–*18*). Determining both the duration of pre-eruption storage and the processes operating from magma assembly to eruption is important to assess whether eruptible magma is readily available or whether magma bodies are noneruptible for most of their lifetime. Current models developed at other volcanoes are inconclusive. Some favor storage at near-solidus temperature or even below solidus, therefore requiring large-scale reheating before eruption to mobilize highly crystalline magmas (*19*–*22*). Others favor prolonged storage in an eruptible state (*17*). Moreover, most of these studies focus on evolved calc-alkaline arc volcanoes, but it remains unclear whether these models are also applicable to alkaline volcanoes such as Somma-Vesuvius.

At Somma-Vesuvius, a single U-Th isochron date obtained from two multigrain garnet fractions and milligram quantities of bulk rock and glass from the 8890-year-old Mercato eruption provides the only evidence for extended pre-eruption storage of phonolite magmas that produce the most voluminous and hazardous eruptions (*23*). This would imply that voluminous melt-rich reservoirs are present for several thousand years before erupting violently. However, these time scales are still significantly shorter than crystal residence times inferred from U-Th isotope systematics of major phenocrysts in phonotephrites of the 1944 eruption (*24*), suggesting that mafic magmas are stored much longer [up to ~40 thousand years (ka)] beneath Vesuvius and/or old crystals are recycled into younger eruptive products. To better constrain the time scales and conditions of phonolite magma storage, we use recently developed techniques that allow in situ U-Th disequilibrium dating of Ca-rich garnet phenocrysts at the subcrystal scale using laser ablation inductively coupled plasma mass spectrometry (LA-ICPMS) (*25*). Combined with detailed textural and geochemical characterization of a subset of U-Th–dated crystals, this provides a comprehensive petrochronology framework for assessing the time scales and dynamics of magma storage beneath Somma-Vesuvius. We integrate

[1]Institute of Geochemistry and Petrology, Department of Earth Sciences, ETH Zurich, Zurich, Switzerland. [2]Dipartimento di Scienze della Terra, Università degli Studi di Milano, Milan, Italy. [3]CNRS, Géosciences Environnement Toulouse, Observatoire Midi-Pyrénées, Toulouse, France. [4]CNRS, Centre de Recherches Pétrographiques et Géochimiques, Vandœuvre les Nancy, France. [5]Dipartimento di Scienze della Terra e Geoambientali, University of Bari, Bari, Italy. [6]Istituto Nazionale di Geofisica e Vulcanologia, Bologna section, Bologna, Italy. [7]CNR, Istituto di Geologia Ambientale e Geoingegneria, Milan, Italy.
*Corresponding author. Email: joern.wotzlaw@gmail.com

our results from Somma-Vesuvius with data from other volcanoes worldwide to investigate variable storage regimes and constrain the processes and parameters controlling the duration of subvolcanic magma storage.

RESULTS

Garnet U-Th isotope systematics

We performed a total of 738 U-Th isotope analyses on both crystal interiors and outermost rims of unpolished garnet crystals from four major Plinian and sub-Plinian eruptions of Somma-Vesuvius (see Materials and Methods for details): The 8890 years before the present (B.P.) Mercato eruption (*26*), the 3950 years B.P. Avellino eruption (*4*, *27*), the AD 79 (Pompeii) eruption (*1*, *2*, *7*), and the AD 472 (Pollena) eruption (*28*, *29*). U-Th isotope systematics of garnet phenocrysts yield well-defined internal isochrons (Fig. 1), providing precise estimates of garnet crystallization ages. The observed spread in (^{238}U)/(^{232}Th), particularly in the case of the Avellino garnets, is, in part, related to small apatite inclusions with low U/Th ratios. These small inclusions are likely related to boundary layer crystallization and are therefore considered isochronous with the garnet host (*30*). This is consistent with isochrons obtained only from inclusion-free analyses, yielding indistinguishable but less precise dates. We therefore do not consider these inclusions to compromise the interpretation of the isochron dates as garnet crystallization ages.

Interior domains of garnet phenocrysts extracted from pumices of the 8890 years B.P. Mercato eruption (*26*) yielded a U-Th isochron date of 14.56 ± 1.25 ka (all uncertainties are 95% confidence intervals including overdispersion; Fig. 1). This is in excellent agreement with the bulk garnet-glass–whole rock isochron date of 14.4 ± 1.1 ka reported by Scheibner *et al.* (*23*). Outermost crystal surfaces of Mercato garnets did not yield sufficient spread in U/Th to calculate a meaningful isochron, but all analyses overlap with the isochron of the crystal interiors. Mercato garnets yielded the lowest initial (^{230}Th)/(^{232}Th) of all analyzed samples (0.823 ± 0.050).

Interior domains of garnet from the 3950 years B.P. Avellino eruption (*4*, *27*) yielded U-Th isochron dates of 8.93 ± 0.29 ka for crystals from the early erupted phonolitic white pumices and 8.81 ± 0.47 ka for crystals from the tephriphonolitic gray pumices. Analyses of outermost crystal surfaces of garnets from the white pumices yielded a U-Th isochron date of 8.01 ± 0.95 ka that is within uncertainty of the crystal interiors but consistent with a younger age based on crystal stratigraphy. Surface analyses of garnets from the gray pumices did not yield a meaningful isochron because of the limited number of analyses, but individual analyses are all overlapping with the interior domain isochron. Avellino garnets from white and gray pumices yielded (^{230}Th)/(^{232}Th) of 0.850 ± 0.011 and 0.830 ± 0.015, respectively (Fig. 1), within uncertainties identical to Mercato garnets.

Garnets from the historic AD 79 Pompeii (*1*, *2*, *7*) and the AD 472 Pollena eruptions (*28*, *29*) yielded indistinguishable U-Th isochron dates. Garnets extracted from the white pumices of the Pompeii eruption yielded a U-Th isochron date of 3.31 ± 0.99 ka, and garnets from the gray pumices yielded an isochron date of 2.82 ± 0.95 ka. Garnets from the Pollena eruption yielded an isochron date of 2.32 ± 1.42 ka that was previously reported by Wotzlaw *et al.* (*25*). While these dates are overlapping within uncertainty, the initial (^{230}Th)/(^{232}Th) is distinct between the Pompeii and Pollena, with Pollena garnets having a significantly higher initial (^{230}Th)/(^{232}Th) (Fig. 1).

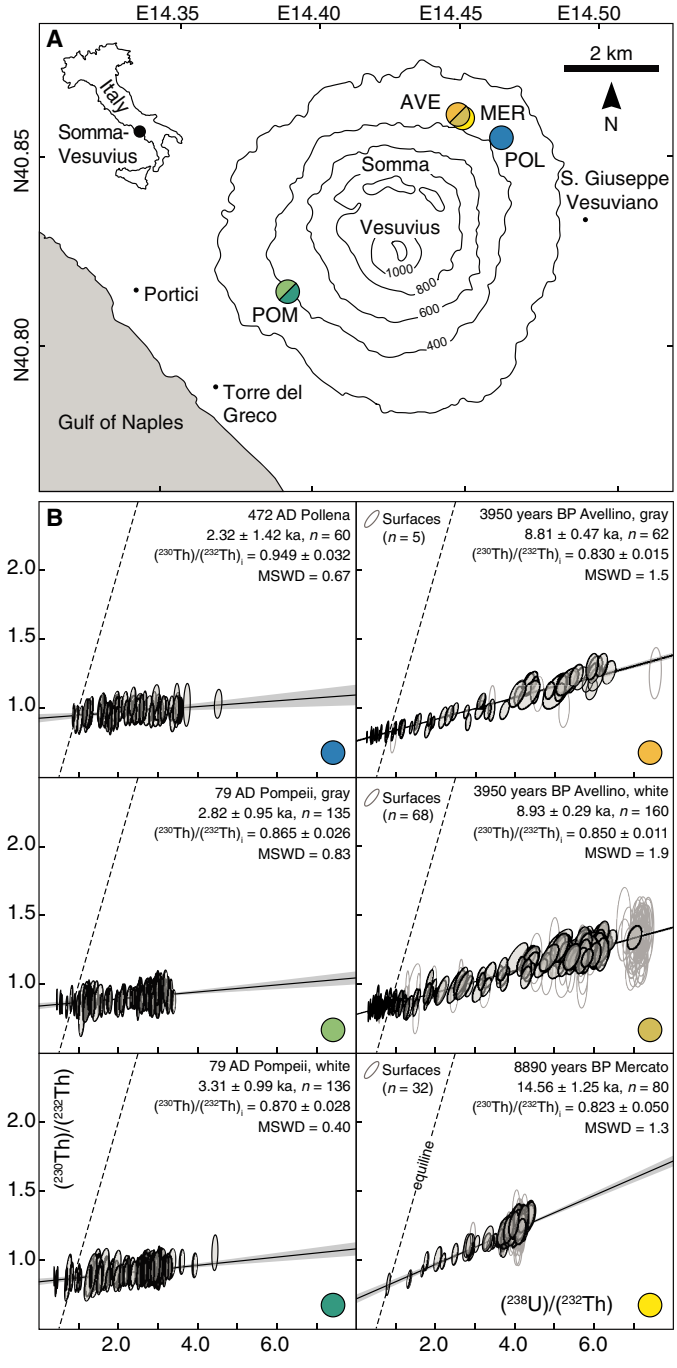

Fig. 1. Map of Mount Somma-Vesuvius and garnet U-Th isotope systematics. (**A**) Location map (*25*) showing sampling localities of sample analyses in this study. MER, Mercato; AVE, Avellino; POM, Pompeii; POL, Pollena. (**B**) U-Th isotope systematics of garnet phenocrysts. Isochron calculations were performed using IsoplotR (*49*). All data are plotted with 2σ analytical uncertainties, and isochron dates and intercepts are reported with 95% confidence intervals including overdispersion. Analyses of outermost crystal surfaces are shown as light gray ellipses but were not included in isochron calculations. All U-Th isotopic data displayed in this figure are provided in table S5. MSWD, mean square weighted deviation.

Major and trace element composition of garnet phenocrysts

Compositional variations of garnet phenocrysts provide insights into magma reservoir dynamics and heterogeneity during garnet growth. Each eruption shows compositionally distinct garnet populations, but garnets from the phonolitic (white) and tephriphonolitic (gray) pumices are compositionally indistinguishable in the geochemically zoned deposits (Fig. 2), suggesting that they crystallized from similar host melts before the development of the compositional layering. Garnets display variations from slightly to strongly fractionated rare earth element (REE) patterns, caused by heavy rare earth element (HREE) concentrations ranging over two orders of magnitude. As garnet controls most of the REE budget in Vesuvius phonolites (*31*), these variations are caused by variable HREE depletion of the melt during crystallization of a garnet-bearing mineral assemblage. Avellino, Pompeii, and Pollena garnets also display moderate Eu anomalies, and the most fractionated garnets are depleted in the lighter HREE (e.g., Er) relative to heavier HREE (Fig. 2), consistent with cocrystallization of feldspar, amphibole, and pyroxene, respectively. Pollena garnets have the least pronounced Eu anomaly because of cocrystallization of leucite instead of sanidine. These observations are in line with phase equilibria experiments (*12*) and inclusions of these minerals in analyzed garnets. Mercato garnets are the least fractionated with respect to HREE depletion, consistent with the crystal-poor nature of the Mercato pumices. They do, however, have the most pronounced Eu anomaly, suggesting that the Mercato magma underwent extensive feldspar fractionation before melt extraction and garnet crystallization.

Garnet phenocrysts of the Mercato eruption are homogeneous with respect to major and trace element composition (Fig. 2) (*31*), consistent with the limited geochemical variability in Mercato pumices (*32*). In contrast, garnets from the Avellino, Pompeii, and Pollena eruptions are compositionally zoned in major and trace elements (Figs. 2 and 3, and fig. S3). These complex zoning patterns reflect large-scale heterogeneities and dynamic compositional fluctuations in the host magmas during magma assembly and crystallization. In our samples of the Avellino, Pompeii, and Pollena eruptions, most garnets have reverse zoning with more HREE depleted cores and less depleted rims (Figs. 2 and 3). This is accompanied by only minor variations in feldspar-compatible elements (e.g., Sr, Eu/Eu*), suggesting that only minor feldspar cocrystallized with garnet (Fig. 2). Comparison of garnet compositions between the different eruptions (fig. S4) shows that trace elements that are not strongly controlled by garnet fractionation (e.g., Sr, Zr, and Eu/Eu*) mirror the progressively less evolved magma compositions throughout the lifetime of the volcano, providing insights into the long-term evolution of the Vesuvius magma plumbing system.

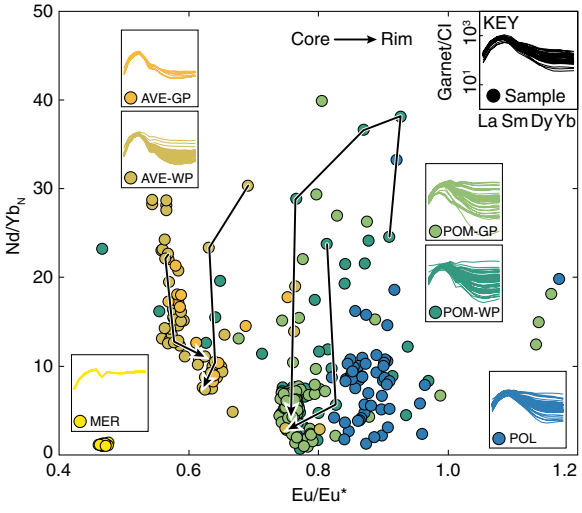

Fig. 2. Trace element composition of garnet phenocrysts from Somma-Vesuvius. Shown are the garnet trace element composition in $(Nd/Yb)_N$ versus Eu/Eu* space. Insets show chondrite-normalized rare earth element patterns. Black arrows connect core-to-rim spot profiles of selected garnet from the Avellino and Pompeii eruptions showing systematic zoning patterns with more evolved (higher Nd/Yb) and more diverse crystal interiors overgrown by more homogeneous and less evolved (lower Nd/Yb) rims. MER, Mercato; AVE, Avellino; POM, Pompeii; POL, Pollena; GP, Grey pumice; WP, White pumice.

DISCUSSION

Time scales and conditions of magma storage before Plinian and sub-Plinian eruptions of Somma-Vesuvius

As garnet is an integral part of the phonolite mineral assemblage and the crystallization sequence is well constrained by experiments (*12*), garnet crystallization ages provide tight constraints on the upper crustal residence time of the phonolitic magmas before eruption. Mean pre-eruption residence times are here computed as the difference between the mean garnet crystallization age and the eruption age (Fig. 4). Garnets from the Mercato eruption crystallized 5.67 ± 1.25 ka before eruption, and garnets from the gray and white pumices of the Avellino eruption record 4.87 ± 0.47 ka and 4.99 ± 0.29 ka of pre-eruption residence time. Garnets from the Pompeii eruption crystallized within 0.91 ± 0.95 ka and 1.40 ± 0.99 ka of the eruption,

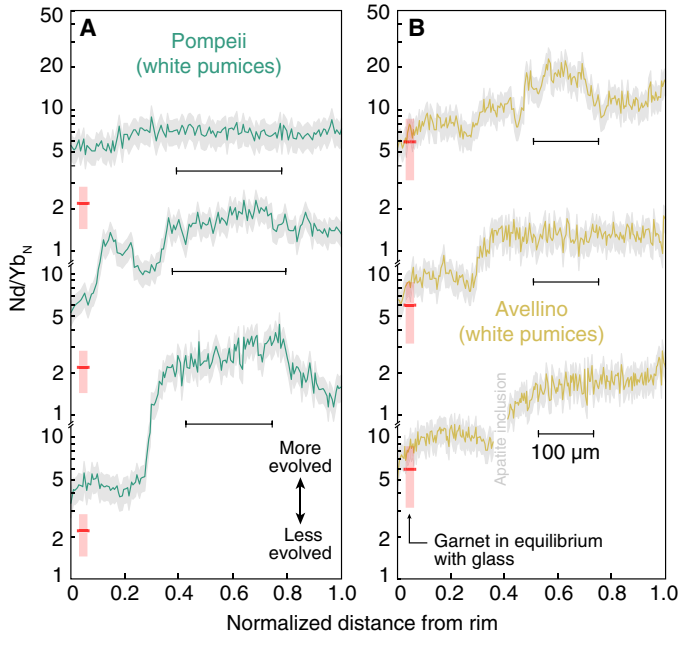

Fig. 3. Trace element profiles of garnet phenocrysts from Somma-Vesuvius. Shown are the selected high-resolution trace element core-rim line profiles measured by LA-ICPMS of Pompeii (**A**) and Avellino (**B**) garnet phenocrysts. Shown are the Nd/Yb ratios as a function of normalized distance from the crystal rim. Red bars are garnet compositions in equilibrium with the host phonolitic glass calculated using partition coefficients derived from Mercato garnet-glass pairs (*31*). Scale bars, 100 µm.

while garnets from the sub-Plinian Pollena eruption crystallized within uncertainty of the eruption age with a computed residence time of 0.81 ± 1.42 ka. We did not find any evidence for recycling of garnets from previous eruptions. We considered this possibility especially for the younger eruptions with overlapping U-Th dates, but Pompeii and Pollena garnets are distinct with respect to their initial Th isotopic and trace element compositions (Figs. 2 and 4, and fig. S4).

Important observations are that the pre-eruption residence times decrease throughout the lifetime of the volcano and that they scale with the progressively shorter repose intervals (Fig. 4). Garnets from the prehistoric Mercato and Avellino eruptions record rather long pre-eruption storage, while the historic Pompeii and Pollena eruptions are preceded by much shorter upper crustal storage. Storage time scales seem to be independent of erupted volume or storage pressure (Fig. 4). The shift to shorter residence times in the two younger eruptions does not coincide with the upward migration of the magma reservoir that is only recorded after the Pompeii eruption (Fig. 4) (*12*, *13*). The shorter residence times of the Pompeii and Pollena garnets can also not be explained by later garnet crystallization in these magmas—at 200 MPa, garnet is stable in Mercato, Avellino, and Pompeii phonolites at temperatures between 780° and 820°C and even at higher temperatures in the Pollena phonolite (*12*). Garnet is also stable over a much larger pressure range in the Pompeii and Pollena phonolites compared to the narrow pressure window of garnet stability in the older eruptions (*12*). Phase equilibria therefore do not explain the shorter garnet residence time in the Pompeii and Pollena magmas. We therefore interpret garnet residence times as directly recording the duration of pre-eruption magma storage in the upper crustal reservoir.

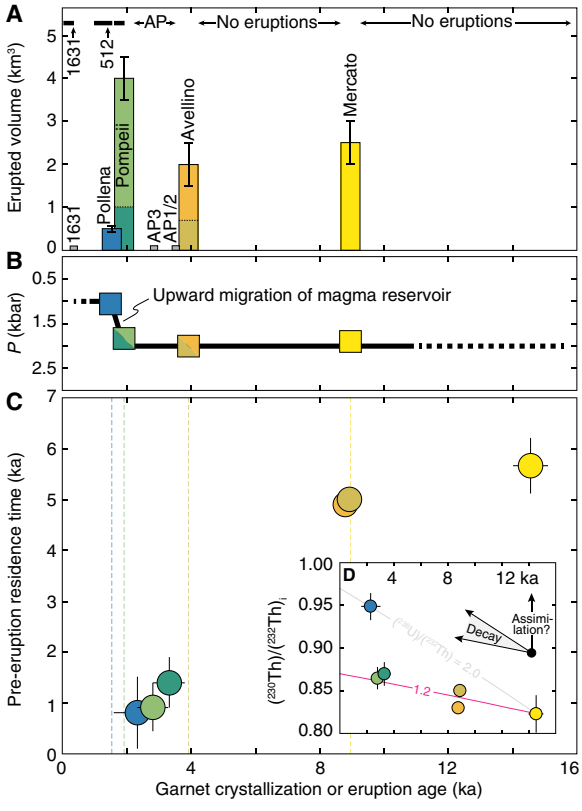

Fig. 4. Comparison of erupted volumes of Somma-Vesuvius phonolites, magma storage pressure, and crystal residence times. (**A**) Estimated erupted volumes of major Plinian and sub-Plinian eruptions of Somma-Vesuvius (*36*). Also shown are the prominent intervals without any record of eruptions preceding the Mercato and Avellino eruptions, the "AP" eruptive interval (*35*), and periods of semipersistent (phono-)tephritic eruptions (black bars) (*36*). (**B**) Storage pressure of Somma-Vesuvius phonolites based on experimental phase equilibria (black line) (*12*) and chlorine solubility (symbols) (*13*). (**C**) Pre-eruption residence time of garnet phenocrysts as a function of garnet crystallization age illustrating the decreasing residence time with decreasing age. Uncertainties are shown as 1σ for clarity. Vertical lines are the corresponding eruption ages. (**D**) Inset shows the initial $(^{230}Th)/(^{232}Th)$ as a function of age. Gray and pink lines illustrate the effect of in situ radioactive decay in a closed system for different $(^{238}U)/(^{232}Th)$ ratios.

Our estimates of upper crustal storage time scales based on garnet U-Th dates are significantly longer than residence time estimates based on sanidine and clinopyroxene crystal size distributions (CSDs) of Somma-Vesuvius phonolites (10^1 to 10^2 years) (*33*) and Ba diffusion in sanidine from the AD 79 eruption (10^1 years) (*11*). Such systematic differences between U-series–derived mineral crystallization ages and time scales based on CSD and trace element diffusion are well documented at other volcanoes (*19*). The hiatus between these chronometers has been interpreted to reflect intervals of magma storage at low temperature followed by rapid remobilization before eruption. However, the short crystal residence times of phonolitic magmas calculated from sanidine crystal sizes have large uncertainties associated with crystal growth rates, and sanidine crystal sizes in our sample of the Avellino eruption are larger (up to ~4-mm length) than those reported by Pappalardo and Mastrolorenzo (*33*) (up to ~1-mm length). This would substantially reduce the discrepancy between the CSD-derived residence times and our garnet crystallization ages. Furthermore, phenocryst CSD time scales reflect the duration of crystal growth independent of the absolute timing relative to the eruption. Time scales based on Ba diffusion in sanidine only record the timing of high-Ba rim growth associated with pre-eruption recharge and cumulate melting (*11*, *34*) while sanidine cores may be resolvably older. The last recharge events that caused the compositional zoning of the magma chamber are not recorded by garnet phenocrysts, but our U-Th dates reveal the longevity of the phonolitic magma in the shallow subvolcanic reservoir.

The last mafic recharge events that caused the compositional layering of the Avellino and Pompeii deposits and presumably triggered these eruptions are not recorded by garnets as all garnets crystallized before the mafic recharge. The reverse zoning patterns of the Avellino and Pompeii garnets, however, suggest that the eruption-feeding magma reservoirs were assembled from progressively less evolved magmas. Garnet cores crystallized from a melt that was more evolved than the white phonolitic pumice glass, while later magma batches were less evolved (Fig. 3). The relationship between garnet rims and their host pumices further provides constraints on the extent of magma mixing during recharge events after garnet crystallization. Garnet rims of the Avellino eruption are close to trace element equilibrium with the phonolitic glass of the white pumice deposits that represent the topmost part of the magma chamber (Fig. 3). In contrast, garnet rims of the Pompeii eruption have more evolved trace element compositions than expected based on published partition coefficients (Fig. 3). This suggests that the upper part of the Avellino phonolite magma was unaffected by the recharge event that caused the compositional layering, while the

recharge event that caused the compositional zoning of the Pompeii deposit also affected the phonolitic top of the reservoir. This is consistent with the larger proportion of "gray" magma in the Pompeii deposits and the less evolved glass composition of the Pompeii phonolite pumices that have distinctly higher Ba, lower Zr, and less fractionated REE patterns compared with Avellino and Mercato pumices (fig. S2). The garnet-glass trace element disequilibrium therefore suggests that the resident phonolitic magma of the Pompeii eruption was similarly evolved as the Avellino and Mercato phonolites before mafic recharge. The fractionated trace element compositions of Pollena garnets (Fig. 2) suggest a similarly evolved phonolitic magma before extensive mafic recharge that affected the entire reservoir to produce the compositionally zoned but predominantly tephriphonolitic magma chamber.

Prolonged phonolite storage controls eruption dynamics

Garnet residence times scale with the progressively shorter repose intervals, suggesting that the phonolite reservoir was refilled rapidly after each eruption and that phonolitic magma was present in the upper crust throughout most of the volcano's lifetime. This is best resolved for the Avellino garnets that are indistinguishable in age from the Mercato eruption (Fig. 4). Pompeii garnets are slightly younger than the Avellino eruption but overlap with the sub-Plinian eruptions of the AP interval (*35*), and Pollena garnets are indistinguishable in age from the Pompeii eruption. The intervals between garnet crystallization and eruption coincide with intervals of volcanic quiescence (*6*, *36*). The only record of volcanic activity between the Mercato and Avellino eruptions are ash layers that have glass compositions more consistent with being derived from Campi Flegrei (*36*). This suggests that the presence of phonolitic magma in the upper crust controlled the eruption dynamics of Somma-Vesuvius by preventing the ascent and eruption of less evolved magmas from deeper crustal reservoirs. Frequent lower-energy mafic eruptions during more recent times suggest that no phonolitic magma was present since the Pollena eruption. Future large-volume Plinian eruptions, often considered the worst-case scenario for future eruptions of Vesuvius (*4*), are therefore unlikely without several centuries of volcanic quiescence. The last eruption of Vesuvius occurred in 1944, and therefore, the volcano has been in repose for almost 80 years. That is still substantially shorter than the repose intervals and magma residence times before most large-volume Plinian and sub-Plinian eruptions (*36*). The laterally extensive seismic attenuation zone detected at about 8-km depth beneath Vesuvius (*37*) might reflect a growing phonolitic magma body as suggested by Scaillet *et al.* (*12*) based on the similarity between the storage depth of previous phonolite magma chambers and the depth of the seismic attenuation zone. However, as the composition of the current magma body beneath Vesuvius is unknown, this seismic attenuation zone may alternatively be part of the tephritic magma supply system. Only future eruptions will reveal the true nature of this magma body, but if it is phonolitic, a large-volume Plinian eruption would likely require a substantially longer repose interval. Smaller-volume sub-Plinian events similar to the AD 1631 eruption are nonetheless possible, as they may not require such extended repose times.

Long-term evolution of the Somma-Vesuvius plumbing system

The time scales of shallow phonolite magma storage derived from garnet U-Th ages are significantly shorter than most crystal residence times in phonotephrites of the 1944 eruption (*24*). U-Th isochrons for major phenocrysts yielded crystal residence times between 12 and 39 ka. Only a groundmass-leucite pair yielded a U-Th age indistinguishable from the eruption age recording either short storage in a shallow subvolcanic magma chamber before eruption or groundmass crystallization during decompression (*24*). The older crystal ages suggest the presence of a deeper-seated and long-lived mafic to intermediate reservoir from which the tephritic lavas and tephras are derived directly whereby old crystals are recycled and scavenged during ascent. The shorter residence times of garnet phenocrysts and their trace element compositions suggest that phonolites are extracted as highly evolved crystal-poor magmas to produce upper crustal chambers that feed Plinian and sub-Plinian eruptions. In the upper crustal reservoir, these evolved phonolites undergo variable degree of crystallization and are substantially modified by later recharge events recorded by compositional and isotopic variations of major mineral phases (i.e., clinopyroxenes and feldspar) and hosted melt inclusions (*7*, *8*, *11*, *27*, *32*). Such a polybaric magma supply system has also been envisioned by Pappalardo and Mastrolorenzo (*33*), but they suggested substantially shorter phonolite storage and differentiation time scales.

Extraction of phonolitic melts from a common long-lived deep reservoir is also reflected in the temporal evolution of the initial Th isotopic composition (Fig. 4D) and garnet trace element compositions (fig. S4). The evolution from the Mercato to Pompeii eruption is consistent with closed-system radioactive decay with a $(^{238}U)/(^{232}Th)$ of 1.2, which is the measured $(^{238}U)/(^{232}Th)$ in Mercato bulk pumices (*23*). Higher initial $(^{230}Th)/(^{232}Th)$ of Pollena garnets requires either a distinct source magma with higher $(^{238}U)/(^{232}Th)$ or assimilation of high U/Th crust such as shallow crustal carbonates. The shift in Th isotope composition from the Pompeii to Pollena eruption coincides with the upward migration of the magma reservoir (Fig. 4) (*12*) into shallow carbonate wall rocks and is consistent with progressively more carbonate assimilation inferred from stable and radiogenic isotopes (*38*, *39*). Most notably, post–472 AD eruptions have more silica-undersaturated compositions and $^{87}Sr/^{86}Sr$ ratios that correlate with trace element ratios indicative of carbonate assimilation (*38*). $^{87}Sr/^{86}Sr$ ratios of phenocrysts further become more radiogenic with decreasing crystallization pressure, reflecting shallow open system behavior (*38*). Because of the large Th isotopic contrast between the carbonate wall rock and the phonolite magma, initial $(^{230}Th)/(^{232}Th)$ ratios are sensitive tracers for carbonate assimilation and may be used more systematically in the future to quantify the impact of such shallow open system behavior at Vesuvius and elsewhere.

Discrete magma storage regimes in subvolcanic magma plumbing systems

The compositional dependence on magma storage times identified at Somma-Vesuvius may be a more general feature of volcanoes worldwide that point toward variable magma storage regimes in volcanic plumbing systems. We expanded a global compilation of U-series–derived crystal residence times (*19*) and compiled the corresponding bulk rock compositions to investigate the relationship between crystal residence time and host magma composition (table S6). We further compiled zircon U-Th data and corresponding host magma compositions from a variety of volcanoes in arc and intraplate settings to assess differences in storage time scales recorded by major phenocrysts compared to accessory minerals (table S7).

The compilation of major phenocryst residence times reveals that crystals from evolved dacitic to rhyolitic and phonolitic magmas

[MgO < 2 weight % (wt %)] predominantly yield short residence times between ~1 and ~10 ka (Fig. 5A). Less evolved andesitic to basaltic magmas yield a much broader range of residence times between <1 and ~100 ka with a mode between 10 and 100 ka. The data distribution in composition versus residence time space of the global dataset strongly resembles the distribution of Somma-Vesuvius phonolites and phonotephrites (Fig. 5A). This similarity allows us to reconcile the global data distribution in the context of variable crustal storage regimes identified at Somma-Vesuvius including (i) ephemeral shallow crustal storage of andesitic to basaltic lavas, (ii) prolonged deep crustal storage of intermediate to mafic mushes from which old crystals are scavenged during ascent and incorporated into younger eruptions, and (iii) upper crustal storage of highly evolved dacitic/rhyolitic and phonolitic magmas after extraction of crystal-poor magma from a deeper crystal mush (Fig. 5A). Compiled major phenocryst U-Th data are from bulk mineral separates comprising hundreds of crystals, while our garnet U-Th dates are from in situ analyses, thereby avoiding averaging crystals with potentially different crystallization ages. The similar residence times of Somma-Vesuvius phonolites and evolved magmas from other volcanoes suggest that recycling of older phenocrysts is less common in the more evolved rocks that are generated by efficient melt extraction from silicic mushes compared with more mafic systems.

Zircon U-Th geochronology–derived residence times appear to increase with increasing MgO of the host magma independent of geodynamic setting (subduction related versus intraplate magmatism; Fig. 5B). Relative to the major phenocryst data, the zircon data from silicic to intermediate rocks are slightly shifted toward longer residence times and data for mafic magmas (>5 wt % MgO) are not available. The latter aspect is easily explained by zircon only saturating in evolved magmas (*40*). The longer zircon residence times for evolved magmas may be explained either by zircon recording a longer crystallization interval or by recycling of older zircons from earlier magma batches. In the most evolved magmas, such as crystal-poor rhyolites and phonolites, the longer median zircon residence times relative to the phenocryst data may indicate incorporation of zircon crystals from the source mush during melt extraction. This is consistent with crystal-poor rhyolites often containing a large number of zircons with crystallization ages close to eruption age [e.g., (*41*, *42*)] and only few resolvably older crystals. Notably, this may not be true for alkaline systems (*15*, *43*), in which zircon does not saturate in the crystal mush before melt extraction (*44*). Therefore, the emerging picture for the most evolved magma compositions appears to be consistent for both the zircon and major phenocryst data as they both suggest relatively short (1 to 10 ka) upper crustal storage times after melt extraction. The longer zircon residence times of less evolved magmas are consistent with these magmas

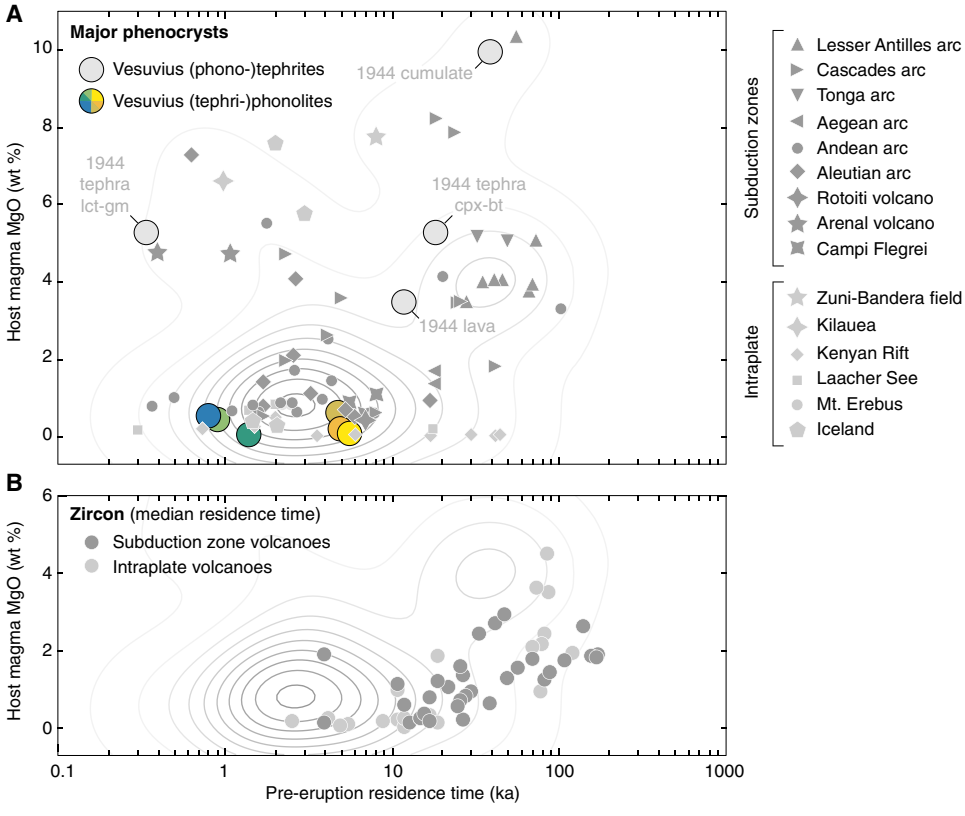

Fig. 5. Time scales of magma storage beneath Somma-Vesuvius and other volcanoes worldwide as a function of magma composition. (**A**) Major phenocryst residence times depending on magma composition. Host magma composition (bulk rock or glass MgO) is plotted as a function of crystal residence time for Somma-Vesuvius phonolites (this study), phonotephrites (*24*), and a global compilation of arc (dark gray) and intraplate (light gray) volcanoes [modified from Cooper and Kent (*19*); table S6]. Gray lines are density contours of a two-dimensional kernel density estimate of the global data compilation. (**B**) Zircon residence times depending on magma composition. Host magma composition is plotted as a function of median zircon residence time for various subduction-related and intraplate volcanoes (table S7). Density contours for the major phenocryst data plotted in (A) are shown for comparison.

representing erupted silicic to intermediate crystal mushes in which zircon records the entire interval of magma assembly, prolonged crystallization, and storage before eruption. The apparent compositional dependence on magma residence times revealed by the data from Somma-Vesuvius and the global data compilation therefore points toward distinct magma storage regimes in crustal-scale magma plumbing systems that feed distinct types of volcanic eruption. This provides a framework for predicting future volcanic activity from past eruptive products and allows assessing future hazards.

MATERIALS AND METHODS

Sampling, garnet separation, and sample preparation

Garnet phenocrysts were extracted from proximal pumice fall deposits (Fig. 1 and fig. S1). Both the Avellino and Pompeii deposits display significant compositional variations with early erupted phonolitic white pumices and later erupted tephriphonolitic gray pumices (fig. S1) (*7*, *27*) that were sampled and processed separately. Garnet was typically more abundant in the more evolved phonolites but was present in all samples of these eruptions. The Pollena tephra deposits are also compositionally zoned but predominantly tephriphonolitic (*28*, *29*). Garnets were separated from various portions of the Pollena deposits and analyzed as a single population. Garnet separation involved gentle crushing of pumices within disposable bags, sieving to <1-mm grain size followed by washing in deionized water and heavy liquid separation in methylene iodide. Adherent matrix glass was removed by ultrasonicating handpicked garnet crystals for 2 min in 8% hydrofluoric acid. Cleaned garnet crystals were mounted in epoxy mounts. Surface U-Th isotope analyses (see below for details) were performed on unpolished crystal faces before polishing. For all other analyses, mounted crystals were polished to expose crystal interiors and imaged using backscattered electron imaging using a JEOL JSM-6390 scanning electron microscope.

Major and trace element analysis of pumice glasses

Complementary major and trace element analyses of host pumice glasses were performed by electron probe microanalysis (EPMA) and LA-ICPMS (tables S1 and S2). Pumice fragments were embedded in 1-inch epoxy discs, characterized by backscattered electron imaging using a JEOL JSM-6390 scanning electron microscope and analyzed for major elements using a JEOL JXA-8230 electron microprobe at ETH Zurich. Analyses of Si, Ti, Al, Fe, Cr, Mg, Mn, Na, Ca, Cl, K, and P were performed with an accelerating voltage of 15 kV and a beam current of 10 nA. To minimize alkali migration during analysis, the beam was defocused to 20 μm, and the counting time was limited to 20 s on peak and 10 s on backgrounds with Si and alkalis measured first in the sequence. NIST610 and NIST612 were analyzed as secondary reference materials to monitor instrumental drift and assess reproducibility.

Trace element concentrations of pumice glasses were determined by LA-ICPMS on the same samples analyzed previously by EPMA using an Australian Scientific Instruments (ASI) Resolution 155 laser ablation system coupled to a Thermo Element XR sector field ICPMS at ETH Zurich. The laser ablation system was operated with a spot size of 29 μm, a repetition rate of 5 Hz, and an on-sample energy density of 3.5 J/cm^2. Trace element concentrations were quantified using NIST612 reference glass as the primary standard. GSD-1G and ATHO-G glasses were analyzed as secondary standards to assess accuracy and reproducibility.

Major and trace element analysis of garnet phenocrysts

Selected garnets from the Pompeii and Pollena eruptions were analyzed for major elements using EPMA (table S3). All analyses were performed using a JEOL JXA-8200 electron microprobe at the Department of Earth Sciences at ETH Zurich using a 15-kV accelerating voltage and a 20-nA beam current. Garnets were analyzed for Si, Al, Ti, Ca, Fe, Mg, Zr, Na, Mn, V, and Y using natural grossular garnet as calibration standard for Si, Ca, and Al; natural andradite garnet for Fe; natural pyrope garnet for Mg; and various natural and synthetic reference materials for the minor elements. In addition, semiquantitative elemental distribution maps (fig. S3) were acquired using the same instrument but at 80-nA beam current. Major element compositions of Avellino and Mercato garnets were previously reported by Scheibner *et al.* (*31*).

Trace element compositions of garnet phenocrysts from all sampled eruptions were determined by LA-ICPMS both on single spots (table S4) and continuous line profiles using an ASI Resolution 155 laser ablation system coupled to a Thermo Element XR sector field ICPMS. For spot analyses, the laser was operated with an energy density of 3.5 J/cm^2, a repetition rate of 5 Hz, and a spot size of 19 μm. The average Ca concentration determined by EPMA (32 wt %) was used as the internal standard, and NIST610 reference glass was used as the primary reference material to correct for elemental fractionation and instrumental drift. Data reduction was performed in SILLS (*45*). Complementary continuous line profiles were measured on selected garnets using the same instrumentation and operating conditions except for a beam diameter of 13 μm to improve spatial resolution. The data were processed for single mass sweeps, and uncertainties on line profiles were estimated from the reproducibility of equivalent line profiles measured on NIST610.

In situ U-Th geochronology of garnet phenocrysts

U-Th isotopic data were acquired by LA-ICPMS using the methods described in detail by Wotzlaw *et al.* (*25*) with a brief summary provided here. Analyses were performed at ETH Zurich using the same instrumentation as for the trace element analyses described above. For analyses of crystal interiors, the laser ablation system was operated with an energy density of 3.5 J/cm^2, a repetition rate of 10 Hz, and a spot size of 163 μm. For crystal surface analyses, the repetition rate was reduced to 2 Hz to improve depth resolution, and two squid smoothing devices (*46*) were coupled to reduce signal fluctuations due to the low repetition rate. The smaller volume of ablated material, however, resulted in lower count rates and consequently lower precision of the surface analyses (Fig. 1). During all analyses, masses 230 and 235 were measured in pulse-counting mode, whereas masses 232 and 238 were measured in analog mode. ^{230}Th count rates were corrected for contributions from the ^{232}Th peak tail using the abundance sensitivity determined from repeat measurements of a high-Th monazite performed during each analytical session (*47*). Instrumental mass bias was determined from the measured ^{238}U/^{235}U relative to the natural U isotopic ratio of 137.818 (*48*). The relative sensitivity factor (RSF) for correcting U-Th elemental fractionation was determined from analyses of the ^{230}Th/^{238}U ratio of a secular equilibrium garnet reference material (Mali garnet) assuming (^{230}Th)/(^{238}U) = 1 [see (*25*) for details]. The average U-Th RSF over the course of this study was 1.14 ± 0.08 (1 SD). All U-Th isotopic data are provided in table S5, and fig. S6 shows results for secular equilibrium garnets analyzed as reference materials. U-Th data for garnets from the Pollena eruption were previously reported by Wotzlaw *et al.* (*25*). Calculations of isochron ages and initial Th isotopic ratios were performed in IsoplotR (*49*).

SUPPLEMENTARY MATERIALS

Supplementary material for this article is available at https://science.org/doi/10.1126/sciadv.abk2184

REFERENCES AND NOTES

1. H. Sigurdsson, S. Cashdollar, S. R. J. Sparks, The eruption of Vesuvius in A.D. 79: Reconstruction from historical and volcanological evidence. *Am. J. Archaeol.* **86**, 39–51 (1982).
2. H. Sigurdsson, S. N. Carey, W. Cornell, T. Pescatore, The eruption of Vesuvius in A.D. 79. *Natl. Geogr. Res.* **1**, 332–387 (1985).
3. C. Principe, J.-C. Tanguy, S. Arrighi, A. Paiotti, M. Le Goff, U. Zoppi, Chronology of Vesuvius' activity from A.D. 79 to 1631 based on archeomagnetism of lavas and historical sources. *Bull. Volcanol.* **66**, 703–724 (2004).
4. G. Mastrolorenzo, P. Petrone, L. Pappalardo, M. Sheridan, The Avellino 3780-yr-B.P. catastrophe as a worst-case scenario for a future eruption at Vesuvius. *Proc. Natl. Acad. Sci. U.S.A.* **103**, 4366–4370 (2006).
5. R. Cioni, A. Bertagnini, R. Santacroce, D. Andronico, Explosive activity and eruption scenarios at Somma-Vesuvius (Italy): Towards a new classification scheme. *J. Volcanol. Geotherm. Res.* **178**, 331–346 (2008).
6. A. Sbrana, R. Cioni, P. Marianelli, R. Sulpizio, D. Andonico, G. Pasquini, Volcanic evolution of the Somma-Vesuvius Complex (Italy). *J. Maps* **16**, 137–147 (2020).
7. R. Cioni, L. Civetta, P. Marianelli, N. Metrich, R. Santacroce, A. Sbrana, Compositional layering and syneruptive mixing of a periodically refilled magma chamber: The A.D. 79 plinian eruption of Vesuvius. *J. Petrol.* **36**, 739–776 (1995).
8. R. Cioni, P. Marianelli, R. Santacroce, Thermal and compositional evolution of the shallow magma chambers of Vesuvius: Evidence from pyroxene phenocrysts and melt inclusions. *J. Geophys. Res. Solid Earth* **103**, 18277–18294 (1998).
9. T. Shea, J. F. Larsen, L. Gurioli, J. E. Hammer, B. F. Houghton, R. Cioni, Leucite crystals: Surviving witnesses of magmatic processes preceding the 79AD eruption at Vesuvius, Italy. *Earth Planet. Sci. Lett.* **281**, 88–98 (2009).
10. L. Pappalardo, G. Buono, S. Fanara, P. Petrosino, Combining textural and geochemical investigations to explore the dynamics of magma ascent during Plinian eruptions: A Somma–Vesuvius volcano (Italy) case study. *Contrib. Mineral. Petrol.* **173**, 61 (2018).
11. D. J. Morgan, S. Blake, N. W. Rogers, B. De Vivo, G. Rolandi, J. P. Davidson, Magma chamber recharge at Vesuvius in the century prior to the eruption of A.D. 79. *Geology* **34**, 845–848 (2006).
12. B. Scaillet, M. Pichavant, R. Cioni, Upward migration of Vesuvius magma chamber over the past 20,000 years. *Nature* **455**, 216–219 (2008).
13. H. Balcone-Boissard, G. Boudon, R. Cione, J. D. Webster, G. Zdanowicz, G. Orsi, L. Civetta, Chlorine as a geobarometer for alkaline magmas: Evidence from a systematic study of the eruptions of Mount Somma-Vesuvius. *Sci. Rep.* **6**, 21726 (2016).
14. J. A. Vazquez, M. R. Reid, Probing the accumulation history of the voluminous Toba magma. *Science* **305**, 991–994 (2004).
15. A. K. Schmitt, Laacher See revisited: High-spatial-resolution zircon dating indicates rapid formation of a zoned magma chamber. *Geology* **34**, 597–600 (2006).
16. L. L. Claiborne, C. F. Miller, D. M. Flanagan, M. A. Clynne, J. L. Wooden, Zircon reveals protracted magma storage and recycling beneath Mount St. Helens. *Geology* **38**, 1011–1014 (2010).
17. M. Barboni, P. Boehnke, A. K. Schmitt, T. M. Harrison, P. Shane, A. S. Bouvier, L. Baumgartner, Warm storage for arc magmas. *Proc. Natl. Acad. Sci. U.S.A.* **113**, 13959–13964 (2016).
18. G. Weber, L. Caricchi, J. L. Arce, A. K. Schmitt, Determining the current size and state of subvolcanic magma reservoirs. *Nat. Commun.* **11**, 5477 (2020).
19. K. M. Cooper, A. J. R. Kent, Rapid remobilization of magmatic crystals kept in cold storage. *Nature* **506**, 480–483 (2014).
20. N. L. Andersen, B. R. Jicha, B. S. Singer, W. Hildreth, Incremental heating of Bishop Tuff sanidine reveals preeruptive radiogenic Ar and rapid remobilization from cold storage. *Proc. Natl. Acad. Sci. U.S.A.* **114**, 12407–12412 (2017).
21. A. E. Rubin, K. M. Cooper, C. B. Till, A. J. R. Kent, F. Costa, M. Bose, D. Gravley, C. Deering, J. Cole, Rapid cooling and cold storage in a silicic magma reservoir recorded in individual crystals. *Science* **356**, 1154–1156 (2017).
22. D. Szymanowski, J. F. Wotzlaw, B. S. Ellis, O. Bachmann, M. Guillong, A. von Quadt, Protracted near-solidus storage and pre-eruptive rejuvenation of large magma reservoirs. *Nat. Geosci.* **10**, 777–782 (2017).
23. B. Scheibner, A. Heumann, G. Wörner, L. Civetta, Crustal residence times of explosive phonolite magmas: U-Th ages of magmatic Ca-Garnets of Mt. Somma-Vesuvius (Italy). *Earth Planet. Sci. Lett.* **276**, 293–301 (2008).
24. S. Black, R. Macdonald, B. DeVivo, C. R. J. Kilburn, G. Rolandi, U-series disequilibria in young (A.D. 1944) Vesuvius rocks: Preliminary implications for magma residence times and volatile addition. *J. Volcanol. Geotherm. Res.* **82**, 97–111 (1998).
25. J. F. Wotzlaw, M. Guillong, A. Balashova, F. Forni, I. Dunkl, H. B. Mattson, O. Bachmann, In-situ garnet ^{238}U-^{230}Th geochronology of Holocene silica-undersaturated volcanic tuffs at millennial-scale precision. *Quat. Geochronol.* **50**, 1–7 (2019).
26. D. Mele, R. Sulpizio, P. Dellino, L. La Volpe, Stratigraphy and eruptive dynamics of a pulsating Plinian eruption of Somma-Vesuvius: The Pomici di Mercato (8900 years B.P.). *Bull. Volcanol.* **73**, 257–278 (2011).
27. R. Sulpizio, R. Cioni, M. A. Di Vito, D. Mele, R. Bonasia, P. Dellino, The Pomici di Avellino eruption of Somma-Vesuvius (3.9 ka BP). Part I: Stratigraphy, compositional variability and eruptive dynamics. *Bull. Volcanol.* **72**, 539–558 (2010).
28. G. Rolandi, R. Munno, I. Postiglione, The A.D. 472 eruption of the Somma volcano. *J. Volcanol. Geotherm. Res.* **129**, 291–319 (2004).
29. R. Sulpizio, D. Mele, P. Dellino, L. La Volpe, A complex, subplinian-type eruption from low-viscosity, phonolitic to tephri-phonolitic magma: The AD 472 (Pollena) eruption of Somma-Vesuvius, Italy. *Bull. Volcanol.* **67**, 743–767 (2005).
30. C. R. Bacon, Crystallization of accessory phases in magmas by local saturation adjacent to phenocrysts. *Geochim. Cosmochim. Acta* **53**, 1055–1066 (1989).
31. B. Scheibner, G. Wörner, L. Civetta, H. G. Stosch, K. Simon, A. Kronz, Rare earth element fractionation in magmatic Ca-rich garnets. *Contrib. Mineral. Petrol.* **154**, 55–74 (2007).
32. M. Aulinas, L. Civetta, M. A. Di Vito, G. Orsi, D. Gimeno, J. L. Fernandez-Turiel, The "Pomici di mercato" Plinian eruption of Somma-Vesuvius: Magma chamber processes and eruption dynamics. *Bull. Volcanol.* **70**, 825–840 (2008).
33. L. Pappalardo, G. Mastrolorenzo, Short residence times for alkaline Vesuvius magmas in a multi-depth supply system: Evidence from geochemical and textural studies. *Earth Planet. Sci. Lett.* **296**, 133–143 (2010).
34. J. A. Wolff, F. Forni, B. S. Ellis, D. Szymanowski, Europium and barium enrichments in compositionally zoned felsic tuffs: A smoking gun for the origin of chemical and physical gradients by cumulate melting. *Earth Planet. Sci. Lett.* **540**, 116251 (2020).
35. D. Andronico, R. Cioni, Contrasting styles of Mount Vesuvius activity in the period between the Avellino and Pompeii Plinian eruptions, and some implications for assessment of future hazards. *Bull. Volcanol.* **64**, 372–391 (2002).
36. R. Santacroce, R. Cioni, P. Marianelli, A. Sbrana, R. Sulpizio, G. Zanchetta, D. J. Donahue, J. L. Joron, Age and whole rock-glass compositions of proximal pyroclastics from the major explosive eruptions of Somma-Vesuvius: A review as a tool for distal tephrostratigraphy. *J. Volcanol. Geotherm. Res.* **177**, 1–18 (2008).
37. E. Auger, P. Gasparini, J. Virieux, A. Zollo, Seismic evidence of an extended magmatic sill under Mt. Vesuvius. *Science* **294**, 1510–1512 (2001).
38. M. Piochi, R. A. Ayuso, B. De Vivo, R. Somma, Crustal contamination and crystal entrapment during polybaric magma evolution at Mt. Somma–Vesuvius volcano, Italy: Geochemical and Sr isotope evidence. *Lithos* **86**, 303–329 (2006).
39. E. M. Jolis, V. R. Troll, C. Harris, C. Freda, M. Gaeta, G. Orsi, C. Siebe, Skarn xenolith record crustal CO_2 liberation during Pompeii and Pollena eruptions, Vesuvius volcanic system, central Italy. *Chem. Geol.* **415**, 17–36 (2015).
40. P. Boehnke, E. B. Watson, D. Trail, T. M. Harrison, A. K. Schmitt, Zircon saturation re-revisited. *Chem. Geol.* **351**, 324–334 (2013).
41. J. F. Wotzlaw, I. N. Bindeman, R. A. Stern, F. X. D'Abzac, U. Schaltegger, Rapid heterogeneous assembly of multiple magma reservoirs prior to Yellowstone supereruptions. *Sci. Rep.* **5**, 14026 (2015).
42. N. L. Andersen, B. S. Singer, M. A. Coble, Repeated rhyolite Eruption from heterogeneous hot zones embedded within a cool, shallow magma reservoir. *J. Geophys. Res. Solid Earth* **124**, 2582–2600 (2019).
43. H. Zou, Q. Fan, H. Zhang, A. K. Schmitt, U-series zircon age constraints on the plumbing system and magma residence times of the Changbai volcano, China/North Korea border. *Lithos* **200-201**, 169–180 (2014).
44. D. Szymanowski, F. Forni, J. A. Wolff, B. S. Ellis, Modulation of zircon solubility by crystal-melt dynamics. *Geology* **48**, 798–802 (2020).
45. M. Guillong, D. L. Meier, M. M. Allan, C. A. Heinrich, B. W. D. Yardley, SILLS: A MATLAB-based program for the reduction of laser ablation ICP-MS data of homogeneous materials and inclusions. *Mineralogical Association of Canada Short Course* **40**, 328–333 (2008).
46. W. Müller, M. Shelley, P. Miller, S. Broude, Initial performance metrics of a new custom-designed ArF excimer LA-ICPMS system coupled to a two-volume laser-ablation cell. *J. Anal. Atom. Spectrom.* **24**, 209–214 (2009).
47. M. Guillong, J. T. Sliwinski, A. K. Schmitt, F. Forni, O. Bachmann, U-Th zircon dating by laser ablation single collector inductively coupled plasma-mass spectrometry (LA-ICP-MS). *Geostand. Geoanal. Res.* **40**, 377–387 (2016).
48. J. Hiess, D. J. Condon, N. McLean, S. R. Noble, ^{238}U/^{235}U systematics in terrestrial uranium-bearing minerals. *Science* **335**, 1610–1614 (2012).
49. P. Vermeesch, IsoplotR: A free and open toolbox for geochronology. *Geosci. Front.* **9**, 1479–1493 (2018).
50. B. R. Jicha, B. S. Singer, B. L. Beard, C. M. Johnson, Contrasting timescales of crystallization and magma storage beneath the Aleutian island arc. *Earth Planet. Sci. Lett.* **236**, 195–210 (2005).
51. M. Touboul, B. Bourdon, B. Villemant, G. Boudon, J. L. Joron, ^{238}U-^{230}Th-^{226}Ra disequilibria in andesitic lavas of the last magamtic eruption of Guadeloupe Soufriere, French Antilles: Processes and timescales of magma differentiation. *Chem. Geol.* **246**, 181–206 (2007).

52. J. Toothill, C. A. Williams, R. Macdonald, S. P. Turner, N. W. Rogers, C. J. Hawksworth, D. A. Jerram, C. J. Ottley, A. G. Tindle, A complex petrogenesis for an arc magmatic suite, St Kitts, Lesser Antilles. *J. Petrol.* **48**, 3–42 (2007).
53. E. Heath, S. P. Turner, R. Macdonald, C. J. Hawkesworth, P. van Calsteren, Long magma residence times at an island arc volcano (Soufriere, St. Vincent) in the Lesser Antilles: Evidence from ^{238}U-^{230}Th isochron dating. *Earth Planet. Sci. Lett.* **160**, 49–63 (1998).
54. E. Heath, R. Macdonald, H. Belkin, C. Hawkesworth, H. Sigurdsson, Magmagenesis at Soufriere Volcano, St Vincent, Lesser Antilles arc. *J. Petrol.* **39**, 1721–1764 (1998).
55. S. Turner, R. George, D. A. Jerram, N. Carpenter, C. Hawkesworth, Case studies of plagioclase growth and residence times in island arc lavas from Tonga and the Lesser Antilles, and a model to reconcile discordant age information. *Earth Planet. Sci. Lett.* **214**, 279–294 (2003).
56. F. J. Tepley III, C. C. Lundstrom, J. B. Gill, R. W. Williams, U-Th-Ra disequilibria and the time scale of fluid transfer and andesite differentiation at Arenal volcano, Costa Rica (1968-2003). *J. Volcanol. Geotherm. Res.* **157**, 147–165 (2006).
57. K. W. W. Sims, R. P. Ackert, F. C. Ramos, R. S. Sohn, M. T. Murrell, D. DePaolo, Determining eruption ages and erosion rates of quaternary basaltic volcanism from combined U-series disequilibria and cosmogenic exposure ages. *Geology* **35**, 471–474 (2007).
58. K. M. Cooper, C. T. Donnelly, in A volcano Rekindled: The First Year of Renewed Eruption at Mount St. Helens, 2004–2006 (D. R. Sherrod, W. E. Scott, P. H. Stauffer, eds.), 827–846, US Geological Survey Professional Paper 1750 (2008).
59. B. R. Jicha, C. M. Johnson, W. Hildreth, B. L. Beard, G. L. Hart, S. B. Shirley, B. S. Singer, Discriminating assimilants and decoupling deep- vs. shallow-level crystal records at Mount Adams using ^{238}U–^{230}Th disequilibria and Os isotopes. *Earth Planet. Sci. Lett.* **277**, 38–49 (2009).
60. B. R. Jicha, G. L. Hart, C. M. Johnson, W. Hildreth, B. L. Beard, S. B. Shirey, J. W. Valley, Isotopic and trace element constraints on the petrogenesis of lavas from the Mount Adams volcanic field, Washington. *Contrib. Mineral. Petrol.* **157**, 189–207 (2009).
61. A. M. Volpe, ^{238}U-^{230}Th-^{226}Ra disequilibrium in young Mt. Shasta andesites and dacites. *J. Volcanol. Geotherm. Res.* **53**, 227–238 (1992).
62. T. L. Grove, S. W. Parman, S. A. Bowring, R. C. Price, M. B. Baker, The role of an H_2O-rich fluid component in the generation of primitive basaltic andesites and andesites from the Mt. Shasta region, N California. *Contrib. Mineral. Petrol.* 142, 375–396 (2001).
63. M. E. Stelten, K. M. Cooper, Constraints on the nature of the subvolcanic reservoir at South Sister volcano, Oregon from U-series dating combined with sub-crystal trace-element analysis of plagioclase and zircon. *Earth Planet. Sci. Lett.* **313-314**, 1–11 (2012).
64. B. Bourdon, G. Wörner, A. Zindler, U-series evidence for crustal involvement and magma residence times in the petrogenesis of Parinacota volcano, Chile. *Contrib. Mineral. Petrol.* **139**, 458–469 (2000).
65. B. R. Jicha, B. S. Singer, B. L. Beard, C. M. Johnson, H. Moreno-Roa, J. A. Naranjo, Rapid magma ascent and generation of ^{230}Th excesses in the lower crust at Puyehue-Cordon Caulle, Southern Volcanic Zone, Chile. *Earth Planet. Sci. Lett.* **255**, 229–242 (2007).
66. P. Ruprecht, K. M. Cooper, Integrating the Uranium-series and elemental diffusion geochronometers in mixed magmas from Volcan Quizapu, Central Chile. *J. Petrol.* **53**, 841–871 (2012).
67. P. Ruprecht, G. W. Bergantz, K. M. Cooper, W. Hildreth, The crustal magma storage system of Volcán Quizapu, Chile, and the effects of magma mixing on magma diversity. *J. Petrol.* **53**, 801–840 (2012).
68. M. K. Reagan, A. M. Volpe, K. V. Cashman, ^{238}U- and ^{232}Th-series chronology of phonolite fractionation at Mount Erebus, Antarctica. *Geochim. Cosmochim. Acta* **56**, 1401–1407 (1992).
69. P. J. Kelly, P. R. Kyle, N. W. Dunbar, K. W. W. Sims, Geochemistry and mineralogy of the phonolite lava lake, Erebus volcano, Antarctica: 1972-2004 and comparison with older lavas. *J. Volcanol. Geotherm. Res.* **177**, 589–605 (2008).
70. G. F. Zellmer, K. H. Rubin, K. Gronvold, Z. Jurado-Chichay, On the recent bimodal magmatic processes and their rates in the Torfajokull-Veidivotn area, Iceland. *Earth Planet. Sci. Lett.* **269**, 387–397 (2008).
71. N. M. Rogers, P. J. Evans, S. Blake, S. C. Scott, C. J. Hawkesworth, Rates and timescales of fractional crystallization from ^{238}U-^{230}Th-^{226}Ra disequilibria in trachyte lavas from Longonot volcano, Kenya. *J. Petrol.* **45**, 1747–1776 (2004).
72. S. Black, R. Macdonald, B. Barreiro, P. N. Dunkley, M. Smith, Open system alkaline magmatism in northern Kenya: Evidence from U-series disequilibria and radiogenic isotopes. *Contrib. Mineral. Petrol.* **131**, 364–378 (1998).
73. A. Heumann, G. R. Davies, U–Th disequilibrium and Rb–Sr age constraints on the magmatic evolution of peralkaline rhyolites from Kenya. *J. Petrol.* **43**, 557–577 (2002).
74. S. Black, R. Macdonald, M. R. Kelly, Crustal origin for peralkaline rhyolites from Kenya: Evidence from U-series disequilibria and Th-isotopes. *J. Petrol.* **38**, 277–297 (1997).
75. K. M. Cooper, M. R. Reid, M. T. Murrell, D. A. Clague, Crystal and magma residence at Kilauea Volcano, Hawaii: ^{230}Th-^{226}Ra dating of the 1955 east rift eruption. *Earth Planet. Sci. Lett.* **184**, 703–718 (2001).
76. G. A. Macdonald, J. P. Eaton, Hawaiian volcanoes during 1955. US Geological Survey Bulletin, 1171, pp. 117 (1964).
77. B. Bourdon, A. Zindler, G. Wörner, Evolution of the Laacher See magma chamber: Evidence from SIMS and TIMS measurements of U-Th disequilibria in minerals and glasses. *Earth Planet. Sci. Lett.* **126**, 75–90 (1994).
78. G. Wörner, H. U. Schmincke, Mineralogical and chemical zonation of the Laacher See tephra sequence (East Eifel, W. Germany). *J. Petrol.* **25**, 805–835 (1984).
79. B. L. A. Charlier, D. W. Peate, C. J. N. Wilson, J. B. Lowenstern, M. Storey, S. J. A. Brown, Crystallization ages in coeval silicic magma bodies: ^{238}U-^{230}Th disequilibrium evidence from the Rotoiti and Earthquake Flat eruption deposits, Taupo Volcanic Zone, New Zealand. *Earth Planet. Sci. Lett.* **206**, 441–457 (2003).
80. R. M. Burt, S. J. A. Brown, J. W. Cole, D. Shelley, T. Waight, Glass-bearing plutonic fragments from ignimbrites of the Okataina caldera complex, Taupo Volcanic Zone, New Zealand: Remnants of a partially molten intrusion associated with preceding eruptions. *J. Volcanol. Geotherm. Res.* **84**, 209–237 (1998).
81. G. Zellmer, S. Turner, C. Hawkesworth, Timescales of destructive plate margin magmatism: New insights from Santorini, Aegean volcanic arc. *Earth Planet. Sci. Lett.* **174**, 265–281 (2000).
82. I. Arienzo, A. Heumann, G. Wörner, L. Civetta, G. Orsi, Processes and timescales of magma evolution prior to the Campanian Ignimbrite eruption (Campi Flegrei, Italy). *Earth Planet. Sci. Lett.* **306**, 217–228 (2011).
83. I. Arienzo, L. Civetta, A. Heumann, G. Wörner, G. Orsi, Isotopic evidence for open system processes within the Campanian ignimbrite (Campi Flegrei, Italy) magma chamber. *Bull. Volcanol.* **71**, 285–300 (2009).
84. J. B. Lowenstern, M. A. Clynne, T. D. Bullen, Comagmatic A-type granophyre and rhyolite from the Alid Volcanic Centre, Eritrea, Northeast Africa. *J. Petrol.* **38**, 1707–1721 (1997).
85. A. K. Schmitt, M. Danisik, N. J. Evans, W. Siebel, E. Kiemele, F. Aydin, J. C. Harvey, Acigöl rhyolite field, Central Anatolia (part 1): High-resolution dating of eruption episodes and zircon growth rates. *Contrib. Mineral. Petrol.* **162**, 1215–1231 (2011).
86. W. Siebel, A. K. Schmitt, E. Kiemele, M. Danisik, F. Aydin, Acigöl rhyolite field, central Anatolia (part II): Geochemical and isotopic (Sr-Nd-Pb, δ^{18}O) constraints on volcanism involving two high-silica rhyolite suites. *Contrib. Mineral. Petrol.* **162**, 1233–1247 (2011).
87. H. Zou, Q. Fan, A. K. Schmitt, J. Sui, U-Th dating of zircons from Holocene potassic andesites (Maanshan volcano, Tengchong, SE Tibetan Plateau) by depth profiling: Time scales and nature of magma storage. *Lithos* **118**, 202–210 (2010).
88. R. T. Tucker, H. Zou, Q. Fan, A. K. Schmitt, Ion microprobe dating of zircons from active Dayingshan volcano, Tengchon, SE Tibetan Plateau: Time scales and nature of magma chamber storage. *Lithos* **172-173**, 214–221 (2013).
89. H. Zou, Z. Guo, Y. Peng, A. K. Schmitt, Q. Fan, Y. Zhao, M. Ma, U-series ages of young volcanoes from the Southeastern Tibetan Plateau: Holocene eruptions and magma evolution timescales. *Lithos* **370-371**, 105643 (2020).
90. S. Harangi, R. Lukacs, A. K. Schmitt, I. Dunkl, K. Molnar, B. Kiss, I. Seghedi, A. Novothny, M. Molnar, Constraints on the timing of Quaternary volcanism and duration of magma residence at Ciomadul volcano, east-central Europe, from combined U-Th/He and U-Th zircon geochronology. *J. Volcanol. Geotherm. Res.* **301**, 66–80 (2015).
91. S. Harangi, K. Molnar, A. K. Schmitt, I. Dunkl, I. Seghedi, A. Novothny, M. Molnar, B. Kiss, T. Ntaflos, P. R. D. Mason, R. Lukács, Fingerprinting the Late Pleistocene tephras of Ciomadul volcano, eastern-central Europe. *J. Quat. Sci.* **35**, 232–244 (2020).
92. T. L. Carley, C. F. Miller, J. L. Wooden, I. N. Bindeman, A. P. Barth, Zircon from historic eruptions in Iceland: Reconstructing storage and evolution of silicic magmas. *Mineral. Petrol.* **102**, 135–161 (2011).
93. A. K. Schmitt, D. F. Stockli, J. M. Lindsay, R. Robertson, O. M. Lovera, R. Kislitsyn, Episodic growth and homogenization of plutonic roots in arc volcanoes from combined U-Th and (U-Th)/He zircon dating. *Earth Planet. Sci. Lett.* **295**, 91–103 (2010).
94. J. M. Lindsay, R. Trumbull, A. K. Schmitt, D. F. Stockli, P. A. Shane, T. M. Howe, Volcanic stratigraphy and geochemistry of Soufrière volcanic centre, Saint Lucia with implications for volcanic hazards. *J. Volcanol. Geother. Res.* **258**, 126–142 (2013).
95. G. Weber, L. Caricchi, J. L. Arce, The long-term life-cycle of Nevado de Toluca Volcano (Mexico): Insights into the origin of petrologic modes. *Front. Earth Sci.* **8**, 563303 (2020).
96. R. G. Popa, M. Guillong, O. Bachmann, D. Szymanowski, B. Ellis, U-Th zircon dating reveals a correlation between eruptive styles and repose periods at the Nisyros-Yali volcanic area, Greece. *Chem. Geol.* **555**, 119830 (2020).
97. A. E. Mucek, M. Danisik, S. de Silva, A. K. Schmitt, I. Pratomo, M. A. Coble, Post-supereruption recovery at Toba caldera. *Nat. Commun.* **8**, 15248 (2017).
98. N. L. Andersen, B. S. Singer, B. R. Jicha, B. L. Beard, C. M. Johnson, J. M. Licciardi, Pleistocene to Holocene growth of a large upper crustal rhyolitic magma reservoir beneath the active Laguna del Maule volcanic field, central Chile. *J. Petrol.* **58**, 85–114 (2017).
99. N. L. Andersen, B. S. Singer, M. A. Coble, Repeated rholite eruption from heterogeneous hot zones embedded within a cool, shallow magma reservoir. *J. Geophys. Res.* **124**, 2582–2600 (2019).

100. E. Klemetti, M. A. Clynne, Localized rejuvenation of a crystal mush recorded in zircon temporal and compositional variation at the Lassen volcanic center, Northern California. *PLOS ONE* **9**, e113157 (2014).
101. M. A. Clynne, L. P. J. Muffler, D. F. Siems, J. E. Taggart Jr., P. Bruggman, Major and EDXRF trace element chemical analyses of volcanic rocks from Lassen Volcanic National Park and vicinity, California. U.S. Geological Survey Open-File Report, Reston, VA, U.S. Geological Survey (2008).

Acknowledgments: We thank D. Szymanowski for help during fieldwork and J. Allaz for technical support during EPMA analyses. This work benefited from insightful and detailed reviews by J. Vazquez and an anonymous reviewer. We further thank B. Schoene for efficient editorial handling and constructive comments. **Funding:** This study received funding from ETH Zurich and the Grubenmann-Burri Fund. **Author contributions:** J.-F.W. conceived the project. J.-F.W., L.B., F.F., and R.S. carried out fieldwork and collected the samples. J.-F.W., L.B., M.G., and O.L. performed LA-ICPMS U-Th isotope and trace element analyses of garnet phenocrysts. J.-F.W. and L.B. performed EPMA analyses of garnet phenocrysts. J.N. carried out major and trace element analyses of glasses from host pumices. J.-F.W. compiled published data, prepared the figures, and wrote the paper. All authors contributed to interpreting the results and editing the manuscript. **Competing interests:** The authors declare that they have no competing interests. **Data and materials availability:** All data needed to evaluate the conclusions in the paper are present in the paper and/or the Supplementary Materials.

Submitted 2 July 2021
Accepted 19 November 2021
Published 12 January 2022
10.1126/sciadv.abk2184

ScienceAdvances

Garnet petrochronology reveals the lifetime and dynamics of phonolitic magma chambers at Somma-Vesuvius

Jörn-Frederik WotzlawLena BastianMarcel GuillongFrancesca ForniOscar LaurentJulia NeukampfRoberto SulpizioCyril Chelle-MichouOlivier Bachmann

Sci. Adv., 8 (2), eabk2184. • DOI: 10.1126/sciadv.abk2184